



Open Archive TOULOUSE Archive Ouverte (OATAO)

OATAO is an open access repository that collects the work of Toulouse researchers and makes it freely available over the web where possible.

This is an author-deposited version published in : <http://oatao.univ-toulouse.fr/>
Eprints ID : 14293

To link to this article : doi: 10.1016/j.nucengdes.2015.07.003
URL : <http://dx.doi.org/10.1016/j.nucengdes.2015.07.003>

To cite this version : Clavier, Rémi and Chikki, Nourdine and Fichot, Florian and Quintard, Michel [Experimental investigation on single-phase pressure losses in nuclear debris beds: Identification of flow regimes and effective diameter](#). (2015) Nuclear Engineering and Design, vol. 292. pp. 222-236. ISSN 0029-5493

Any correspondence concerning this service should be sent to the repository administrator: staff-oatao@listes-diff.inp-toulouse.fr

Experimental investigation on single-phase pressure losses in nuclear debris beds: Identification of flow regimes and effective diameter

R. Clavier^{a,*}, N. Chikhi^{a,**}, F. Fichot^b, M. Quintard^{c,d}

^a Institut de Radioprotection et de Sûreté Nucléaire (IRSN) – PSN-RES/SEREX/LE2M, Cadarache bât. 327, 13115 St Paul-lez-Durance, France

^b Institut de Radioprotection et de Sûreté Nucléaire (IRSN) – PSN-RES/SAG/LEPC, Cadarache bât. 700, 13115 St Paul-lez-Durance, France

^c Université de Toulouse – INPT – UPS – Institut de Mécanique des Fluides de Toulouse (IMFT), Allée Camille Soula, F-31400 Toulouse, France

^d CNRS – IMFT, F-31400 Toulouse, France

H I G H L I G H T S

- Single-phase pressure drops versus flow rates in particle beds are measured.
- Conditions are representative of the reflooding of a nuclear fuel debris bed.
- Darcy, weak inertial, strong inertial and weak turbulent regimes are observed.
- A Darcy–Forchheimer law is found to be a good approximation in this domain.
- A predictive correlation is derived from new experimental data.

A B S T R A C T

During a severe nuclear power plant accident, the degradation of the reactor core can lead to the formation of debris beds. The main accident management procedure consists in injecting water inside the reactor vessel. Nevertheless, large uncertainties remain regarding the coolability of such debris beds. Motivated by the reduction of these uncertainties, experiments have been conducted on the CALIDE facility in order to investigate single-phase pressure losses in representative debris beds. In this paper, these results are presented and analyzed in order to identify a simple single-phase flow pressure loss correlation for debris-bed-like particle beds in reflooding conditions, which cover Darcian to Weakly Turbulent flow regimes.

The first part of this work is dedicated to study macro-scale pressure losses generated by debris-bed-like particle beds, i.e., high sphericity (>80%) particle beds with relatively small size dispersion (from 1 mm to 10 mm). A Darcy–Forchheimer law, involving the sum of a linear term and a quadratic deviation, with respect to filtration velocity, has been found to be relevant to describe this behavior in Darcy, Strong Inertial and Weak Turbulent regimes. It has also been observed that, in a restricted domain ($Re = 15$ to $Re = 30$) between Darcy and Weak Inertial regimes, deviation is better described by a cubic term, which corresponds to the so-called Weak Inertial regime.

The second part of this work aims at identifying expressions for coefficients of linear and quadratic terms in Darcy–Forchheimer law, in order to obtain a predictive correlation. In the case of monodisperse beds, and according to the Ergun equation, they depend on the porosity of the medium, empirical constants and the diameter of the particles. Applicability of the Ergun equation for debris-bed-like particle beds has been investigated by assessing the possibility to evaluate equivalent diameters, i.e., characteristic length allowing correct predictions of linear and quadratic terms by the Ergun equation. It has been observed that the Sauter diameter of particles allows a very precise prediction of the linear term, by less than 10% in most cases, while the quadratic term can be predicted using the product of the Sauter diameter and a sphericity coefficient as an equivalent diameter, by about 15%.

* Corresponding author. Tel.: +33 4 42 19 93 67.

** Corresponding author. Tel.: +33 4 42 19 97 79.

E-mail addresses: remi.clavier@irsn.fr (R. Clavier), nourdine.chikhi@irsn.fr (N. Chikhi).

Nomenclature

Latin letters

D	bed diameter	$93.96 \pm 0.04 \text{ mm}$	(mm)
d	spherical particle diameter		(m)
$d_{(n)}$	number mean diameter	$\sum_i d_i n_i$	(m)
$d_{(l)}$	length mean diameter	$\sum_i d_i^2 n_i$	(m)
$d_{(s)}$	surface mean diameter	$\sum_i n_i d_i$	(m)
$d_{(v)}$	volume mean diameter	$\sum_i d_i^3 n_i$	(m)
d_{St}	Sauter diameter	$\frac{6V_{part}}{S_{part}}$	(m)
d_S	surface equivalent diameter	$\left(\frac{S_{part}}{\pi}\right)^{1/2}$	(m)
d_V	volume equivalent diameter	$\left(\frac{6V_{part}}{\pi}\right)^{1/3}$	(m)
d_i	diameter of i -th sort of particle in a multi-sized spherical particle bed		(m)
H	Bed height	$499.0 \pm 1.6 \text{ mm}$	(mm)
h_K	Ergun constant for permeability		(-)
h_η	Ergun constant for passability		(-)
K	permeability		(m ²)
m_w	mass of water necessary to fill the bed up		(kg)
n_i	number of particle of i -th sort in a multi-sized spherical particle bed		(-)
P	pressure		(Pa)
Q	volumetric flow		(m ³ /s)
Re_p	Reynolds number in porous medium	$\frac{\rho U d_{St}}{\mu(1-\varepsilon)}$	(-)
S_{part}	total surface of particles of a bed		(m ²)
s_{part}	surface of a single particle of a bed		(m ²)
s_i	surface of i -th sort of particle in a multi-sized spherical particle bed		(m ²)
V_{part}	total volume of particles of a bed		(m ³)
v_{part}	volume of a single particle of a bed		(m ³)
v_i	volume of i -th sort of particle in a multi-sized spherical particle bed		(m ³)
U	filtration velocity	$\frac{Q}{\pi D^2/4}$	(m/s)

Greek letters

ε	porosity	(-)
η	passability	(m)
μ	fluid dynamic viscosity	(Pa s)
ρ	fluid density	(kg/m ³)
ρ_w	water density	(kg/m ³)
ψ	sphericity	$\frac{\pi^{1/3}(6V_{part})^{2/3}}{S_{part}}$ (-)

1. Introduction

In the course of a severe nuclear accident, the heat up of the core after complete or partial dry-out can lead to a collapse of fuel assemblies and to the formation of a debris bed, which is much more difficult to cool down than the intact fuel assemblies. This phenomenon has been observed in the TMI-2 highly damaged core in 1979 (Broughton et al., 1989), and reproduced in many experimental programs: LOFT (Hobbins and McPherson, 1990), PHEBUS (Repetto, 1990), PBF (Petti et al., 1989). Removal of the decay heat from the debris bed by reflooding is essential for the mitigation of the accident. However, the success of this operation can be compromised by many factors, such as decay heat power, exothermal oxidation of Zirconium by steam, or a too weak permeability of the

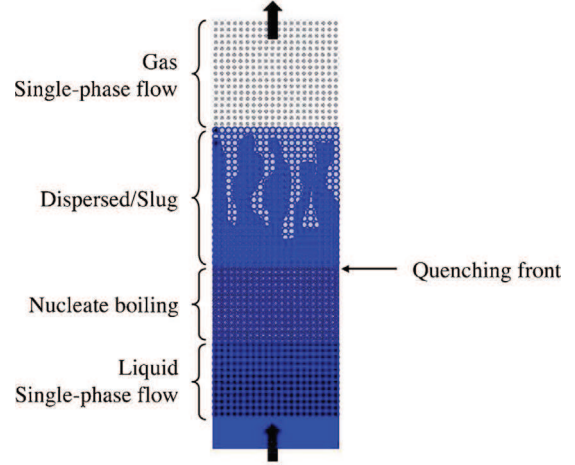


Fig. 1. Schematic view of flow structure in debris beds during reflooding.

bed, and cannot be predicted on the basis of current knowledge and understanding. This implies to study how water penetrates this degraded geometry, which can be described as a hot porous medium.

Many analytical experimental programs have been, and still are dedicated to that question. Tutu et al. (1984) and Ginsberg et al. (1986) performed the first small scale experiments (18 kg of debris) on reflooding of single-size spherical particle beds, i.e., monodisperse beds. Experiments of Wang and Dhir (1988), and, later, the SILFIDE program by EdF (Atkhen and Berthoud, 2006), allowed to reach larger scales (70 kg of debris) and to simulate residual power by an induction heating. During the late-2000s, more representative conditions were investigated during experiments of DEBRIS (Rashid et al., 2008), POMECO (Li and Ma, 2011a,b) and PRELUDE (Repetto et al., 2011) programs, where higher temperatures, up to 1000 °C, were investigated, as well as multi-dimensional effects, for example by use of a lateral by-pass to simulate the effect of non-degraded assemblies in the outer parts of the core. Nowadays, the PEARL program (Chikhi, 2014) aims at investigating the effect of higher temperatures, larger scales and pressure.

In this framework, a new facility, CALIDE, has been built at IRSN (Cadarache, France), in order to study pressure losses generated in representative debris beds in reflooding conditions. The relevance of this study lies in the fact that pressure losses constitute a key parameter governing water penetration in a hot debris bed, and that no consensus exists on correlations valid for beds packed with coarse and/or multi-sized particles (Ozahi et al., 2008; Li and Ma, 2011a,b; MacDonald et al., 1991). Establishment of accurate correlations for pressure losses in porous media are therefore necessary for interpretation of reflooding experiments and their numerical simulation with severe accident codes. Both single and two-phase flow correlations are needed, since both these configurations occur in a hot particle bed during reflooding (see Fig. 1): two-phase flows occur near the quenching front, while single-phase flows, steam or liquid water, occur in upstream and downstream parts. In this work, experimental results obtained with single-phase flows in the CALIDE facility will be analyzed in order to derive a simple macro-scale correlation for single-phase pressure losses validated for porous media representative of nuclear debris beds, and for flowing conditions representative of a reflooding.

A detailed description of the CALIDE facility and of the studied particle beds are provided in Section 2. The CALIDE facility is designed to reproduce the characteristic filtration velocities during reflooding, which basically correspond to Reynolds numbers

ranging from $Re = 15$ to $Re = 100$ in liquid parts, and to $Re \approx 1000$ in gas parts (Repetto et al., 2011), Reynolds number being defined by:

$$Re = \frac{d_{St} U \rho}{\mu (1 - \varepsilon)}, \quad (1)$$

where ρ and μ are the density and dynamic viscosity of the fluid, respectively, ε is the porosity of the medium, and U and d_{St} are the characteristic speed and dimension. U is the filtration velocity, or the Darcy velocity, defined as:

$$U = \frac{Q}{\pi D^2 / 4}, \quad (2)$$

where Q is the volumetric flow, and D the diameter of the test section. The characteristic dimension d_{St} is the Sauter diameter of the particles, defined by:

$$d_{St} = \frac{6V_{part}}{S_{part}}, \quad (3)$$

where V_{part} and S_{part} are the total volume and surface of the particles, respectively.

Many definitions exist for Reynolds number in porous media. The expression used in this work (Eq. (1)), and in particular the $1/(1 - \varepsilon)$ factor, is obtained during the derivation of the Ergun equation from the Kozeny model (du Plessis and Woudberg, 2008). It has been used in similar situations (Ozahi et al., 2008; Li and Ma, 2011a,b).

Experimental particle beds are chosen to be representative of real debris beds, which basically consist in coarse convex particles of size ranging from a few hundred microns to approximately 10 mm, with average porosity of 40% (Chikhi et al., 2014).

Flowing conditions during reflooding are beyond the validity domain of the Darcy's law, which only holds in the creeping regime, up to Reynolds number of a few units to a dozen, depending on the medium (Chauveteau and Thirriot, 1967; Mei and Auriault, 1991; Lasseux et al., 2011). In a macroscopically isotropic medium through which a one-dimensional upward flow occurs, Darcy's law can be expressed as:

$$-\frac{\partial P}{\partial z} + \rho g = \frac{\mu}{K} U, \quad (4)$$

where P is the pressure, g the gravity acceleration, and K the permeability of the medium. When the fluid velocity increases, deformation of the streamlines occur in largest pores, followed by local recirculations, due to pore-scale inertial effects, then progressively in smaller and smaller pores, as shown by Chauveteau and Thirriot (1967). Similarly, for Reynolds numbers of a few hundreds or thousands (Dybbbs and Edwards, 1989; Latifi et al., 1989; Kuwahara et al., 1998), pore-scale turbulence appears. Macroscopically, it results in deviations to Darcy's law, or so-called Forchheimer effects (Forchheimer, 1901), which are often represented by the following mathematical form:

$$-\frac{\partial P}{\partial z} + \rho g = \frac{\mu}{K} U + bU^n. \quad (5)$$

The value of exponent n depends on flow regime and pore-scale geometrical structure. Its determination for CALIDE debris beds is the purpose of Section 3. In structured distillation packings, for example, Soulaire and Quintard (2014) observed $n = 3/2$, while a quadratic deviation ($n = 2$) usually fits well with experimental data for Strong Inertial regime in disordered spherical particle beds (Forchheimer, 1901; Ergun, 1952; MacDonald et al., 1979; Li and Ma, 2011a,b), as well as numerical simulations (Lasseux et al., 2008, 2011). Furthermore, it can be mathematically derived from Navier–Stokes equations, using homogenization method (Mei and Auriault, 1991; Wodié and Levy, 1991; Firdouss et al., 1997), that the first deviations to Darcy's law should fit with a cubic

law ($n = 3$), which corresponds to the so-called “Weak Inertial” regime. Although supported by numerical simulations (Lasseux et al., 2011; Yazdchi and Luding, 2012), the occurrence of Weak Inertial regime in disordered particle beds has never been experimentally observed, to our knowledge, because of the very low magnitude of the cubic term, which is usually lost in measurement uncertainties. This explains why a quadratic law is usually considered as an accurate description of deviations to Darcy's law from Darcy to Turbulent regimes in this class of media. Nevertheless, and given the high precision of the instrumentation of the CALIDE facility, the existence of Weak Inertial regime is worth investigating, especially considering the lack of experimental data concerning that question in the literature.

Quantitative prediction of pressure losses necessitates expressions for coefficients of linear and non-linear terms. In this work, expressions for Darcy (linear) and Strong Inertial (quadratic) terms will be determined. Most often, as it will be discussed later, cubic deviations do not play a significant role, given their magnitude and the range of Reynolds numbers encountered in practice. For that reason, no expression will be sought for coefficient of the cubic term in Weak Inertial regime.

In the case of monodisperse beds, a validated model for pressure losses is the Ergun's law (Ergun, 1952), widely used in chemical and petroleum engineering (Nemec and Levec, 2005; Shaban and Khan, 1995):

$$-\frac{\partial P}{\partial z} + \rho g = \frac{\mu}{K} U + \frac{\rho}{\eta} U^2, \quad (6)$$

where η is the “passability” of the medium, permeability and passability being calculated by:

$$K = \frac{\varepsilon^3 d^2}{h_K (1 - \varepsilon)^2} \quad (7)$$

$$\eta = \frac{\varepsilon^3 d}{h_\eta (1 - \varepsilon)}, \quad (8)$$

where ε is the porosity of the bed, d the diameter of the particles and h_K and h_η are the Ergun constants.

Eqs. (7) and (8) are empirical correlations established for monodisperse beds. In Section 4, their applicability to debris-bed-like media will be investigated, by assessing the possibility to define equivalent diameters, i.e., characteristic dimensions allowing correct predictions of permeability and passability terms when injected in Eqs. (7) or (8). Although physically meaningless, this kind of approach has been found to be relevant, from an empirical point of view, for permeability prediction of this class of media (Chikhi et al., 2014). In this work, different equivalent diameters will be sought for permeability (d_K) and passability (d_η), among available values of literature (Ozahi et al., 2008; Li and Ma, 2011b).

2. CALIDE

2.1. Experimental facility

The CALIDE facility, as illustrated in Fig. 2, is an air/water loop at room temperature and pressure. Its instrumentation allows measurement of pressure losses versus flow-rates in a 93.96 ± 0.04 mm diameter cylindrical test section that contains a particle bed. Six radial holes uniformly distributed along the section allow pressure tapping at different levels inside, downstream and upstream the debris bed. A stainless steel wire mesh is placed at the bottom of the test section to support the bed. A mark is drawn on the test section 499.0 ± 1.6 mm above the bottom wire mesh and is used to adjust the bed height.

Particles are chosen to be representative of nuclear fuel debris, in terms of size and shape, and are presented in next paragraph.

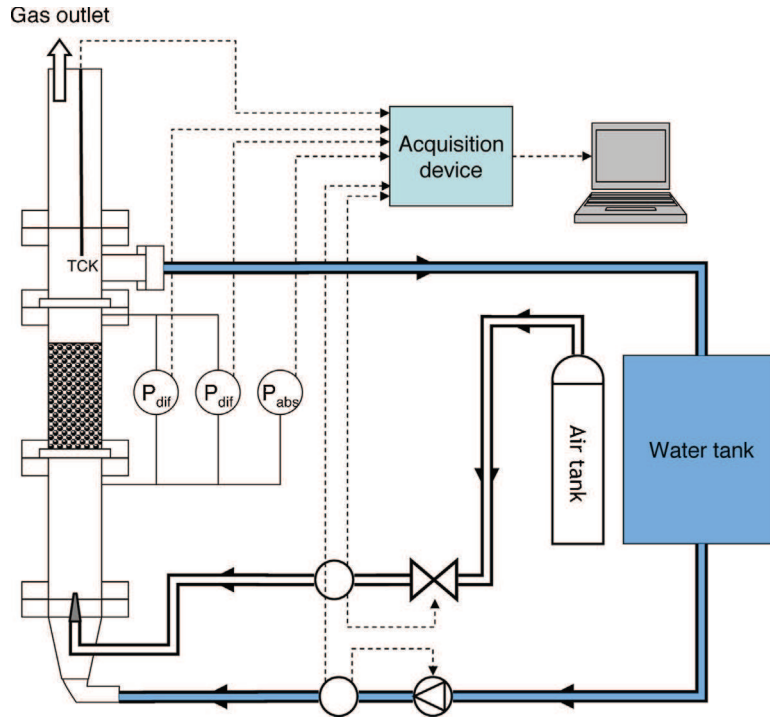


Fig. 2. Schematic representation of the CALIDE facility.

Water and gas flow rates are determined so that filtration velocity is representative of water or steam filtration velocity during a reflooding of a debris bed. According to the Probabilistic Safety Analysis (Durin et al., 2013), reflooding of a debris bed is most likely to occur at a primary pressure ranging from 1 to 10 bar. For this pressure range, the amount of water that can be provided by the safety injection system in a French 1300 MWe PWR ranges between 1300 m³/h and 200 m³/h, which corresponds to filtration velocity of between 32 mm/s and 5 mm/s (the diameter of the vessel is 3.76 m). Evaluation of flowing conditions in the gas phase requires an assumption on steam flowrate. In PRELUDE experiments (Repetto et al., 2013), steam productions up to 100 g/s have been observed for reflooding velocities of 5 mm/s, which corresponds to a steam filtration velocity of 7.2 m/s.

Thus, instrumentation allows measurements of air flows (up to 1000 NI/min ± 0.5% ≃ 2.58 m/s at 20 °C, 1 atm), water flows (up to 600 kg/h ± 0.2% ≃ 24 mm/s), pressure drops (up to 200 mbar ± 0.04%), absolute pressure and fluid temperature. Range and accuracy of each sensor used in CALIDE are listed in Table 1. Air flows, water flows and pressure drops are measured using respectively three air flow-meters-regulating valves (small, medium and large range), two water flow-meters commanding two regulated pumps (small and large range) and two differential pressure sensors (small and large range). Using several sensors for fluid flows and pressure drops was found to be necessary in order to minimize measurement uncertainties at both low and high flow rates.

A thermocouple and an absolute pressure sensor measure the temperature in the test section, which is considered as uniform, and the absolute pressure at the bottom of the debris bed, in order to determine the physical properties of the fluid. Density and viscosity of water are determined from tabulated values (Lide, 1990) and temperature. The viscosity of the air is deduced from the temperature, using the Sutherland law (Lide, 1990), and its density is determined from the perfect gas law:

$$\rho = \frac{P - \Delta P/2}{rT}, \quad (9)$$

where P is the absolute pressure, ΔP is the pressure loss in the debris bed, T the absolute temperature and r the specific gas constant, which is equal to 287 for air. Density is calculated for the average pressure in the debris bed $P - \Delta P/2$ to account for the gas compressibility (report to Appendix for more details).

2.2. Particle beds

An exhaustive state-of-the-art on debris bed granulometry can be found in Chikhi et al. (2014). In this part, the main results of that study are summarized.

Fuel pellets naturally crack during normal operation (Olander, 1990). The size and shape of debris were investigated by experimental programs, like LOFT (Hobbins and McPherson, 1990), PHEBUS (Repetto, 1990) or PBF (Petti et al., 1989) and examination of the debris bed formed in the TMI-2 damaged core (Akers et al., 1986). From the cracking model of Oguma (Oguma, 1983) and literature review, Coindreau et al. (2013) estimated that the shape of the fuel fragments should be similar to prisms and that their sizes should range from 2.4 mm to 3.2 mm as long as the fuel burn-up remains under 40 GWd/tU, and that very thin particles are not produced or do not remain into the bed (up to 30 μm particles could appear beyond this value, by the fragmentation of the high burn-up structures).

The size of fuel fragments in TMI-2 core ranges from 0.3 mm to 4 mm, and its average value is of the order of 2 mm (Akers et al., 1986). This is consistent with the results of LOFT and PBF programs (Chikhi et al., 2014). Concerning cladding particles, it can be calculated (Coindreau et al., 2013) that their average Sauter diameter ranges from 1.1 mm to 1.7 mm.

The porosity of the TMI-2 debris bed has been determined by Akers et al. (1986), and has been found to range from 0.35 to 0.55. An average value of 0.4 is usually used for safety analysis, and for moderately irradiated fuel, for example by Bürger et al. (2006).

Geometry of debris beds is different when created from re-solidification of molten materials falling in liquid water. Granulometry of this kind of debris beds has been investigated by many

Table 1
Instrumentation used on the CALIDE facility.

(a) Flow-meters				
Name		Range	Accuracy	
Air flow	BRONKHORST® F-201-CV	0–10 NI/min	0.5% × Reading	
	BRONKHORST® F-202-AV	0–200 NI/min	+0.1% × Range	
	BRONKHORST® F-203-AV	0–1000 NI/min		
Water flow	BRONKHORST® Cori-Flow M14	0–30 kg/h	0.2% × Reading	
	BRONKHORST® Cori-Flow M55	0–600 kg/h		
(b) Pressure sensors				
Name		Range	Max. range (MR)	Accuracy
Diff	ROSEMOUNT® 3051	–1–7 mbar	±14.19 mbar	0.045% × MR
	ROSEMOUNT® 3051	–10–200 mbar	±1246 mbar	0.04% × Reading +0.023% × MR
Abs	ROSEMOUNT® 3051	0–2 bar	55.2 bar	0.025% × Range

experimental programs on steam explosions. Although the average size of particle is comparable with in-core debris, ranging from 1 mm (Huhtiniemi et al., 1997; Huhtiniemi and Magallon, 1999) to 5 mm (Spencer et al., 1994), the size distribution is much wider. For example, sizes varying from 0.25 to more than 10 mm have been observed in the FARO experiments (Magallon and Huhtiniemi, 2001). Porosity of this kind of bed has been observed to be higher than fuel debris beds, ranging from 0.50 to almost 0.70 (Chikhi et al., 2014). But Ma and Dinh (2010) pointed out that particles, in that case, present an important internal porosity, which leads to overestimate the effective porosity. Thus, these values should not be considered as references.

Therefore, the size of the debris ranges from a few hundred microns to approximately 10 mm. Porosity of debris beds ranges from 35% to 55%.

As explained in the introduction, particle beds studied in CALIDE are designed to be representative of nuclear debris beds. They are presented in Table 2. Non-spherical particle beds and mixtures of spherical particles have been studied.

Non spherical particles (Table 2) consist in three kinds of cylinders and two kinds of prisms. Their dimensions are of the order of fuel pellets fragments. For each kind of particle, geometrical characteristics (diameter, side length, height, surface, volume) have been determined from samples of 10 particles. Diameters and heights have been measured with a caliper, prisms length and particle surface have been determined from picture analysis, and particle volumes have been determined by the water displacement method, which also allowed to measure the particle densities. Table 3(a) summarizes porosity of each bed for air and water experiments.

Nominal sizes of spherical particles range from 1.5 mm to 8 mm. For each size, actual diameters have been measured with a caliper in 4 directions for each one of a 30 particles representative sample. The obtained mean values and standard deviations are summarized in Table 2. Multi-sized spherical particle beds have been considered, in order to study the effect of size distribution on pressure losses. Table 3(b) summarizes the composition and porosity of each mixture.

2.3. Determination of porosity

Pressure loss is very sensitive to porosity. The adopted method consists in determining the volume of the pores by measuring the

mass of water m_w that is necessary to fill it up. The bed height is precisely adjusted on a reference mark situated $H = 499.0 \pm 1.6$ mm above the bottom supporting wire mesh. Knowing the diameter D of the test section, porosity can then be determined by:

$$\varepsilon = \frac{m_w 4}{\rho_w \pi D^2 H}. \quad (10)$$

Porosities of each bed are summarized in Table 3(a) and (b). They range from 35% to 40%, which fits the average porosity of debris beds.

3. Identification of single-phase flow regimes in particle beds

As explained in the introduction, Darcy's law only holds in creeping regime, for Reynolds numbers lower than a limit value ranging from 1 to 10 (Chauveteau and Thirriot, 1967; Mei and Auriault, 1991; Lasseux et al., 2011). For higher Reynolds numbers, modifications in pore-scale flow structure lead to a deviation to Darcy's law, or Forchheimer effects. In non-structured particle beds, this deviation is usually admitted to be quadratic. However, it has been shown, by theoretical considerations and by numerical simulations, that this is an approximation and that deviation to Darcy's law should be cubic (Wodié and Levy, 1991; Firdaouss et al., 1997; Lasseux et al., 2011; Yazdchi and Luding, 2012). This assertion has never been confirmed by experimental observations, to our knowledge, in disordered porous media. In this section, an investigation on the form of deviations to Darcy's law is proposed for particle beds representative of nuclear debris beds.

3.1. Darcy regime

Darcy regime is characterized by a linear dependence between pressure losses and filtration velocity:

$$-\frac{\partial p}{\partial z} + \rho g = \frac{\mu}{K} U, \quad (11)$$

where K is the permeability of the medium. Equation 11 is equivalent to:

$$\frac{\mu U}{-\frac{\partial p}{\partial z} + \rho g} = K. \quad (12)$$

Table 2

Spherical and non-spherical particles used in CALIDE experiments. Materials are glass for spherical particles and porcelain for non spherical particles.

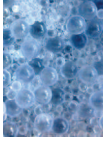


			Diameter (mm)	Density (kg/m ³)			
Spheres	1.5		1.574 ± 0.031	2574.0 ± 7.4			
	2		2.086 ± 0.033	2568.0 ± 7.4			
	3		2.940 ± 0.044	2560.0 ± 7.4			
	4		4.058 ± 0.031	2560.0 ± 7.4			
	8		7.877 ± 0.116	2568.0 ± 7.4			
		Diameter/side (mm)	Height (mm)	Surface (mm ²)	Volume (mm ³)	Density (kg/m ³)	
Cylinders	5 × 5		5.13 ± 0.08	4.53 ± 0.23	114.1 ± 4.2	97.89 ± 0.55	2572.0 ± 7.4
	5 × 8		4.86 ± 0.08	7.39 ± 0.37	150.3 ± 6.7	140.46 ± 0.51	3046.0 ± 8.8
	8 × 12		7.99 ± 0.10	11.13 ± 0.48	380 ± 11	575.5 ± 2.9	2568.0 ± 7.4
Prisms	4 × 4		4.15 ± 0.11	3.84 ± 0.13	69.8 ± 1.1	41.55 ± 0.55	2568.0 ± 7.4
	6 × 6		6.11 ± 0.15	5.87 ± 0.19	156.8 ± 4.1	144.2 ± 1.0	2452.0 ± 7.1

Table 3

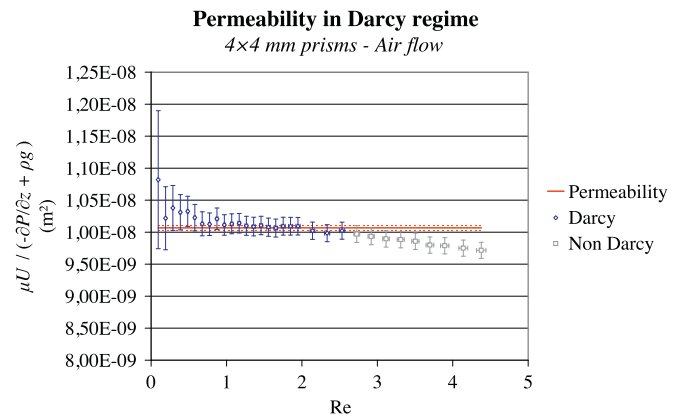
Characteristics of particle beds. Different beds, although packed with the same particles, have been used for air and water experiments, which explains why porosity can be slightly different in air and water flows.

(a) Non-spherical particles							
Cylinder	Flowing fluid		ε				
5 × 5	Air		0.3525 ± 0.0041				
	Water		0.3525 ± 0.0041				
5 × 8	Air		0.3954 ± 0.0047				
	Water		0.3843 ± 0.0045				
8 × 12	Air		0.3855 ± 0.0053				
	Water		0.3642 ± 0.0065				
Prism	Flowing fluid		ε				
4 × 4	Air		0.3646 ± 0.0041				
	Water		0.3750 ± 0.0064				
6 × 6	Air		0.3699 ± 0.0065				
	Water		0.3666 ± 0.0065				
(b) Mixtures of spherical particles							
Mixture number	1.5 mm (%w)	2 mm (%w)	3 mm (%w)	4 mm (%w)	8 mm (%w)	Flowing fluid	ε
1	68.81	-	*-	21.05	10.14	Air	0.3592 ± 0.0064
						Water	0.3592 ± 0.0064
2	59.48	-	28.28	12.24	-	Air	0.3526 ± 0.0039
						Water	0.3646 ± 0.0038
3	-	43.95	-	40.07	15.98	Air	0.3542 ± 0.0049
						Water	0.3578 ± 0.0064
4	38.69	36.95	22.64	1.06	0.67	Air	0.3592 ± 0.0064
						Water	0.3587 ± 0.0064

Thus, the left hand side term of Eq. (12) should be constant and equal to the permeability when Darcy regime occurs. Then it should progressively decrease when inertial effects appear. Fig. 3 shows its evolution in the case of 4 × 4 mm prisms in air flow. Except for very low Reynolds numbers, where measurement uncertainties cause an important noise, Darcy regime is clearly identified up to a limit value of 2.5, approximately.

Precise determination of this limit is not obvious, since the magnitude of Forchheimer effects around this point is below measurement uncertainties. An arbitrary criterion is used here, and consists in verification that the permeability, identified by application of least square fitting between pressure losses and filtration velocity corresponding to diamond symbols in Fig. 3, and represented by the continuous line, must be included within the uncertainty range of all values of expression (12) in Darcy regime.

Similar behaviors are observed for all particle beds in this study, and for air and water flows, and are summarized in Fig. 4(a)–(d). For reasons of clarity, evolution of expression (12) is shown in Darcy regime only, up to apparition of Forchheimer effects. Thus, Darcy's law constitutes a rigorous description of macroscale behavior of

**Fig. 3.** Evolution of expression (12) at low Reynolds number for 4 × 4 mm prisms in air flow. Its value is constant for $Re < 2.5$.

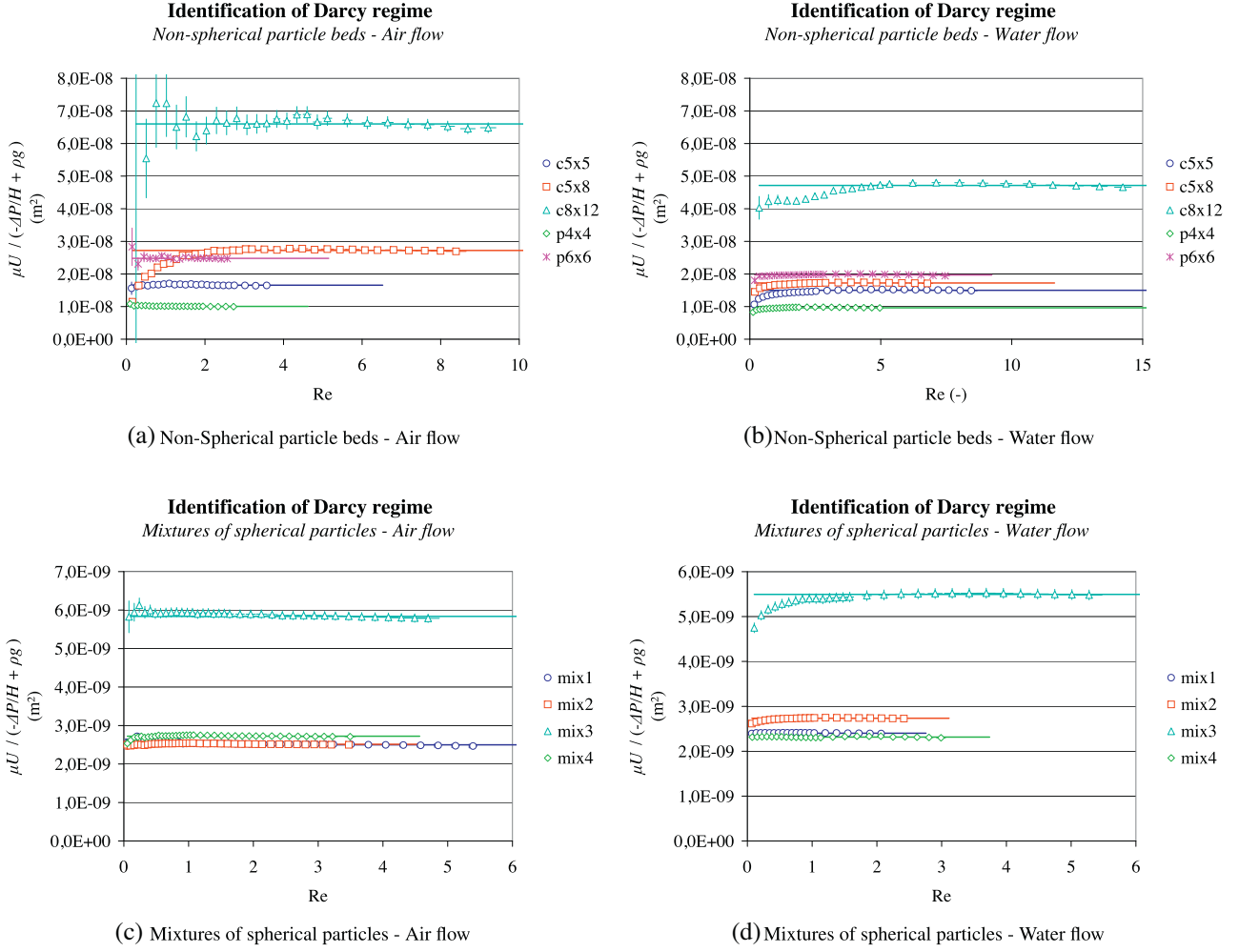


Fig. 4. Identification of Darcy regime for beds packed with non-spherical particles and multi-sized spherical particles. For each bed, the value of the permeability identified with least square method is plotted as constant continuous lines. $c5 \times 5$ means $5 \text{ mm} \times 5 \text{ mm}$ cylinders, $p4 \times 4$ means $4 \text{ mm} \times 4 \text{ mm}$ prisms, mix1 means mixture n°1 in Table 3(b), etc.

pressure losses, except at very low Reynolds number for certain particle beds, where permeability is significantly smaller. This kind of “pre-darcy” regime, which is not supported by any theoretical development, requires further analysis. However, the authors point out that it occurs at small Reynolds numbers, where pressure losses are very weak (of the order of 1 Pa). Therefore, it could be caused by an experimental error, for example an unforeseen singular pressure drop, or a drift of the pressure sensor.

The limit Reynolds number for Darcy’s regime, in these experiments, ranges between 2 ($4 \times 4 \text{ mm}$ prisms in air flow, Fig. 4(a)) and 15 ($8 \times 12 \text{ mm}$ cylinders in water flow, Fig. 4(b)), which is consistent with literature (Chauveteau and Thirriot, 1967; Mei and Auriault, 1991; Lasseux et al., 2011).

This study also allowed to determine the permeabilities of the tested particle beds, which will be used in next paragraphs to determine the deviation to Darcy’s law at higher Reynolds numbers, and in Section 4 to identify a correlation for permeability of the tested particle beds.

3.2. Weak inertial regime

As explained in the introduction, first pore-scale inertial effects should result in a cubic deviation to Darcy’s law, which corresponds to the Weak Inertial regime:

$$-\frac{\partial P}{\partial z} + \rho g = \frac{\mu}{K} U + bU^3. \quad (13)$$

The Weak Inertial regime has been theoretically derived from Navier–Stokes equations using the Homogenization method (Mei and Auriault, 1991; Wodié and Levy, 1991; Firdaouss et al., 1997) and reproduced by numerical simulations (Lasseux et al., 2011; Yazdchi and Luding, 2012), but never observed experimentally in disordered particle beds. Indeed, experimental observation is very difficult, because of the very low magnitude of the cubic deviation, which is lost in measurement noise. Nevertheless, and given the high precision of the instrumentation of the CALIDE facility, the existence of Weak Inertial regime in tested particle beds is worth investigating, especially considering the lack of experimental data on that question.

Eq. (13) is equivalent to a linear dependence between deviation to Darcy’s law and Reynolds number power 3:

$$-\frac{\partial P}{\partial z} + \rho g - \frac{\mu}{K} U = bU^3 = b'Re^3, \quad (14)$$

or, equivalently, to a linear dependence between deviation to Darcy’s law, normalized by the Darcy term, and Reynolds number squared:

$$\frac{-\frac{\partial P}{\partial z} + \rho g - \frac{\mu}{K} U}{\frac{\mu}{K} U} = \frac{bU^3}{\frac{\mu}{K} U} = \frac{bK}{\mu} U^2 = b''Re^2. \quad (15)$$

Fig. 5 is a log–log plot of normalized deviations to Darcy’s law for $4 \times 4 \text{ mm}$ prisms with Reynolds number. Deviations emerge from

Deviations to Darcy law at moderate Reynolds number
4x4 mm prisms - Water flow

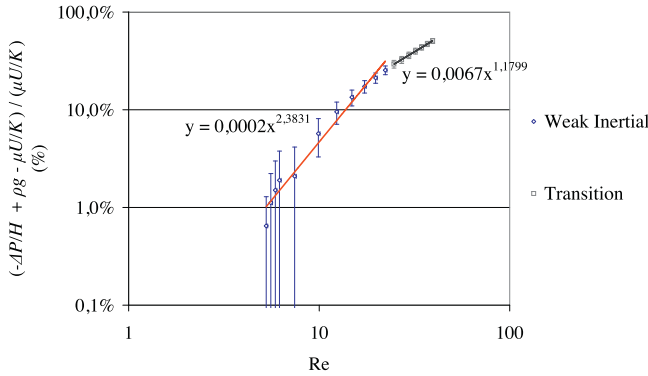


Fig. 5. Normalized deviations to the Darcy's law versus Reynolds number in the case of 4 × 4 mm prisms in water flow.

experimental noise beyond $Re > 10$, and fit with a power law of exponent 2.4. A change of behavior is observed around $Re = 20$, the slope of the correlation dropping from 2.4 to 1.2 beyond that point, which is much closer to the expected value in case of quadratic deviations to Darcy's law, which is 1.

Similar behavior has been observed for all particle beds, in air and water flow. Results are summarized in Fig. 6(a)–(d). First deviations to Darcy's law fit with power laws of exponents ranging from

1.6 to 3.3 and globally close to 2 (expressions are given in the legend of the graphs). Beyond a limit value for Reynolds number, which depends on the medium but ranges from 5 to 50 approximately, the slope of the correlation drops to a value close to 1. However, and for reasons of clarity, data are not shown beyond that limit in Fig. 6(a)–(d).

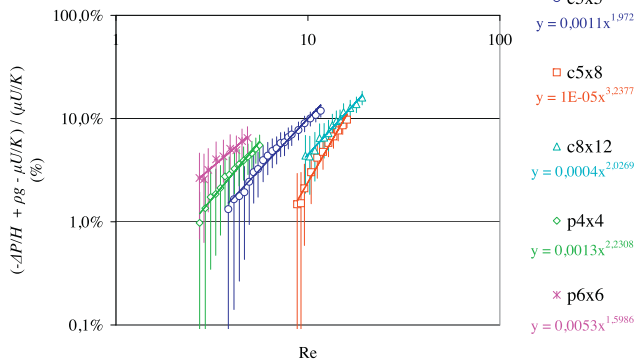
This shows that deviations to Darcy's law significantly differ from the quadratic law as long as Reynolds number remains below certain limits, and that they can be described by power laws of exponents globally of the order of 2. This supports the existence of the Weak Inertial regime in disordered particle beds, and Eq. (13) seems plausible to describe the behavior of pressure losses in that regime. However, it should be pointed out that measurement uncertainties are quite large, because of the weakness of the magnitude of the Weak Inertial deviations, and that further studies should be conducted on that question.

3.3. Strong inertial regime

A quadratic deviation to Darcy's law usually fits well with experimental data at high Reynolds numbers in disordered particle beds (Forchheimer, 1901; Ergun, 1952; MacDonald et al., 1979; Nemeč and Levec, 2005; Ozahi et al., 2008; Li and Ma, 2011a), which corresponds to the Strong Inertial regime, as opposed to the Weak Inertial regime:

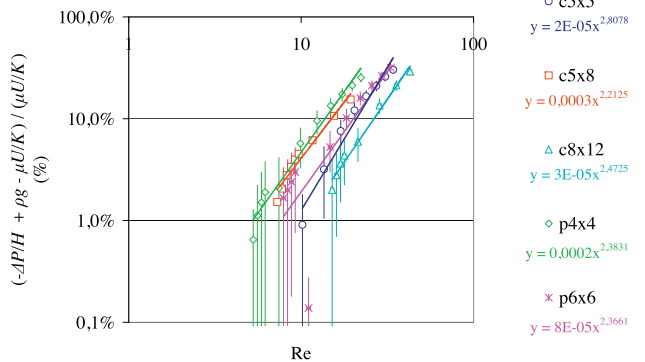
$$-\frac{\partial P}{\partial z} + \rho g = \frac{\mu}{K} U + \frac{\rho}{\eta} U^2. \quad (16)$$

Deviations to Darcy law at moderate Reynolds number
Non-spherical particle beds - Air flow



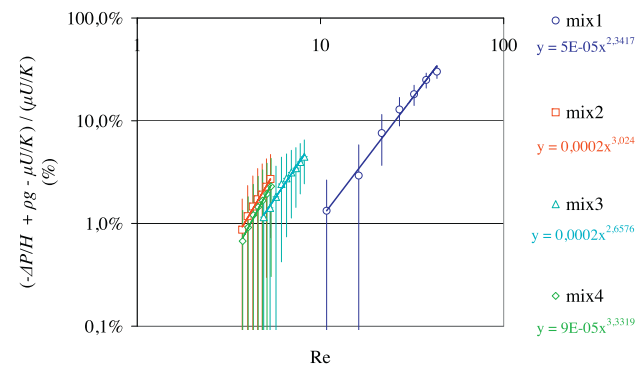
(a) Non-Spherical particle beds - Air flow

Deviations to Darcy law at moderate Reynolds number
Non-spherical particle beds - Water flow



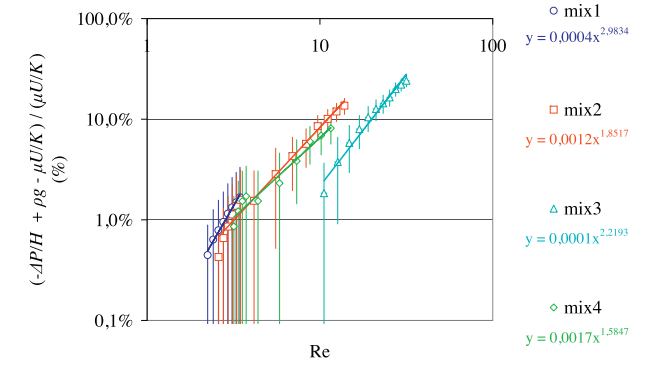
(b) Non-Spherical particle beds - Water flow

Deviations to Darcy law at moderate Reynolds number
Mixtures of spherical particles - Air flow



(c) Mixtures of spherical particles - Air flow

Deviations to Darcy law at moderate Reynolds number
Mixtures of spherical particles - Water flow



(d) Mixtures of spherical particles - Water flow

Fig. 6. Normalized deviations to Darcy's law in Weak Inertial regime versus Reynolds number.

Identification of Strong Inertial regime
8x12 mm cylinders - Water flow

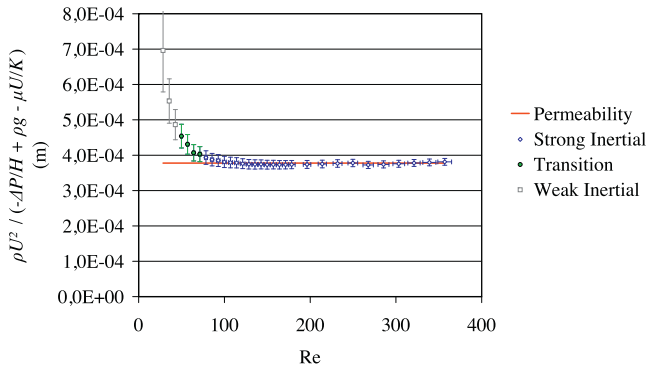


Fig. 7. Evolution of expression (17) versus Reynolds number for 8 × 12 mm cylinders in water flow between Weak Inertial regime and maximum flow velocity. Its value is constant for $Re > 80$.

Verification of the applicability of this equation to the bed tested in this study will be made by using a method analog to the one used in Darcy regime in Section 3.1, which consists in studying the evolution with Reynolds number of the expression:

$$\frac{\rho U^2}{-\frac{\partial P}{\partial z} + \rho g - \frac{\mu}{K} U}, \quad (17)$$

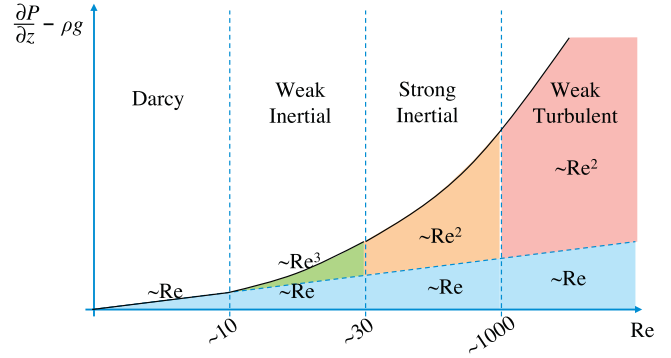
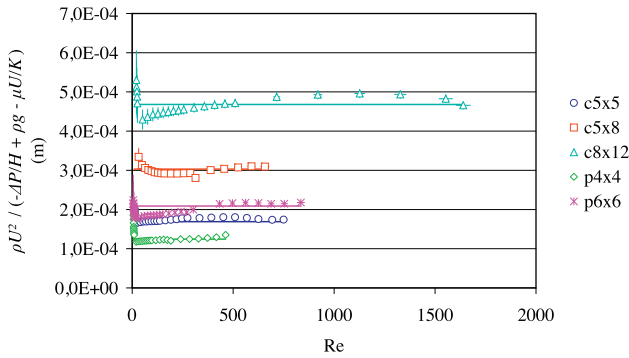


Fig. 8. Schematical evolution of the behavior of pressure losses in particle beds.

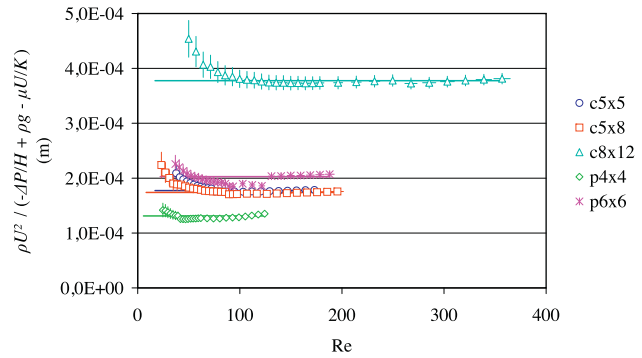
which should be constant and equal to the passability η if Eq. (16) is verified. Fig. 7 presents the evolution of expression (17) with Reynolds number between Weak Inertial regime and maximum flow velocity observed in that study, for 8 × 12 mm cylinders in water flow. A constant value is observed for $Re > 80$, which means that Eq. (16) is verified, and so that deviations to Darcy can be described by a quadratic law in that domain. It has been shown that these deviations fit with a cubic law in Weak Inertial regime, which applies between Darcy regime and $Re < 50$ in that case. Between $Re = 50$ and $Re = 80$, neither cubic nor quadratic law fits with experimental data. This corresponds to the “transition” regime in Fig. 7.

Identification of Strong Inertial regime
Non-spherical particle beds - Air flow



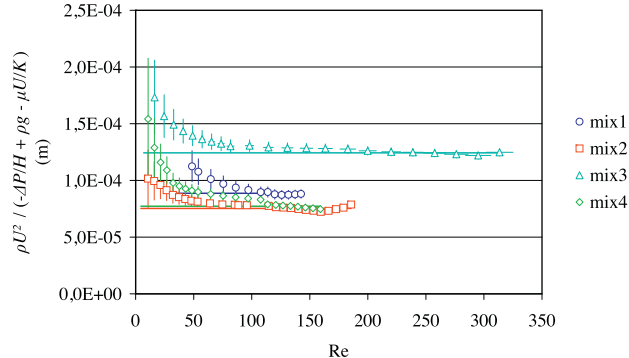
(a) Non-Spherical particle beds - Air flow

Identification of Strong Inertial regime
Non-spherical particle beds - Water flow



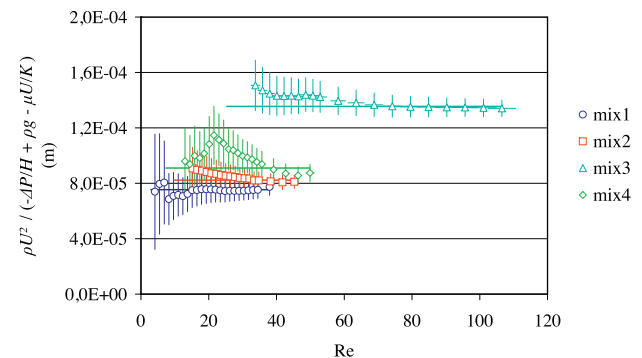
(b) Non-Spherical particle beds - Water flow

Identification of Strong Inertial regime
Mixtures of spherical particles - Air flow



(c) Mixtures of spherical particles - Air flow

Identification of Strong Inertial regime
Mixtures of spherical particles - Water flow



(d) Mixtures of spherical particles - Water flow

Fig. 9. Identification of Strong Inertial regime.

Similar behaviors, summarized in Fig. 9(a)–(d), are observed for each particle bed. Expression (17) is found to be almost constant over a large range of Reynolds number, which means that a quadratic law is relevant to describe deviations to Darcy's law in the Strong Inertial Regime. Since no significant change of behavior is observed for Reynolds numbers of several hundred, where weak pore-scale turbulence, at least, should occur, we may conclude that the validity domain of this approximation can be extended to Weak Turbulent regimes.

3.4. Discussion

At this point, pressure losses generated by non-spherical particle beds and mixtures of spherical particle beds in single-phase air and water flows have been measured in the CALIDE experimental facility. These measurements allowed to identify 3 flow regimes (Fig. 8): Darcy regime, which is characterized by a linear relationship between pressure losses and filtration velocity or Reynolds number, Weak Inertial regime, characterized by a cubic deviation to Darcy's law, and Strong Inertial regime, characterized by a quadratic deviation to Darcy's law. Transition Reynolds numbers between these regimes depend on the medium but seem to be, for the observed particle beds, of the order of $Re \approx 10$ for transition between Darcy and Weak Inertial regime, and of the order of $Re \approx 30$ for transition between Weak Inertial and Strong Inertial regimes. These experiments do not give information about apparition of turbulence, but weak turbulence, at least, should occur for Reynolds numbers of several hundred, *a fortiori* for $Re \approx 1000$. However, no significant difference was observed in the macro-scale behavior of pressure losses between Strong Inertial and Weak Turbulent regimes. Therefore, applicability of quadratic law to describe deviations to Darcy's law can be extended to Weak Turbulent regime, at least for the type of medium considered in this analysis.

It should also be pointed out that deviations to Darcy's law in Weak Inertial regimes are small compared to the Darcy term (30% at maximum, in Fig. 6(b)), and sometimes even smaller than measurement uncertainties. Thus, describing Weak Inertial term by a quadratic law, instead of a cubic law, does not lead to an important error on the total pressure loss prediction. For that reason, and for simplicity of use in practical applications or codes, quadratic deviation to Darcy's law will be considered as a good approximation, also in the Weak Inertial regime.

Therefore, Eq. (16) is relevant in Weak Inertial, Strong Inertial and Weak Turbulent regimes. Furthermore, since the quadratic term becomes negligible before the Darcy term for small velocities, its validity can obviously be extended to the Darcy regime.

Establishment of a predictive correlation now requires expressions for permeability and passability, which range over more than one order of magnitude. This is the objective of the next section.

4. Single-phase pressure losses correlation in particle beds

In previous sections, it has been established that pressure losses in the studied particle beds can be accurately described by:

$$-\frac{\partial P}{\partial z} + \rho g = \frac{\mu}{K} U + \frac{\rho}{\eta} U^2, \quad (18)$$

where K and η are characteristics of the medium called permeability and passability, respectively. Permeabilities and passabilities have been experimentally determined for non-spherical particle beds and multi-sized spherical particle beds, and for air and water flows. Results are summarized in Table 5, for non-spherical particle beds, and in Table 6, for multi-sized spherical particle beds.

As said in the Introduction, expressions for permeability and passability have been proposed by Ergun (1952), in the case of monodisperse beds, i.e., single-sized spherical particle beds:

$$K = \frac{\varepsilon^3 d^2}{h_K (1 - \varepsilon)^2} \quad (19)$$

$$\eta = \frac{\varepsilon^3 d}{h_\eta (1 - \varepsilon)}, \quad (20)$$

where ε is the porosity of the bed, d the diameter of the particles and h_K and h_η two empirical parameters called the Ergun constants. The objective of this section is to investigate the applicability of these expressions to the non-monodisperse beds studied in this work, by assessing the possibility to define equivalent diameters, defined as the dimension that allows a correct prediction of permeability or passability by Eqs. (19) and (20). Although physically meaningless if one consider the upscaling of Navier–Stokes equations, this kind of approach has been found relevant, from an empirical point of view, to predict permeability of debris-bed-like media (Chikhi et al., 2014). It is proposed here to extend this concept to non-Darcy flows. Thus, permeabilities and passabilities of tested particle beds will be expressed as:

$$K = \frac{\varepsilon^3 d_K^2}{h_K (1 - \varepsilon)^2} \quad (21)$$

$$\eta = \frac{\varepsilon^3 d_\eta}{h_\eta (1 - \varepsilon)}, \quad (22)$$

where d_K and d_η are the equivalent diameters for permeability and passability, respectively. It should be noted that d_K and d_η may be *a priori* different.

4.1. Ergun constants

There is little dispersion on values of Ergun constants in literature. Ergun (1952) recommended $h_K = 150$ and $h_\eta = 1.75$, while MacDonald et al. (1979) preferred $h_K = 180$ and $h_\eta = 1.8$. Ozahi et al. (2008) observed $h_K = 160$ and $h_\eta = 1.61$ for high Reynolds flows (800 → 8000). Thus, recommended values for h_K and h_η may vary by more than 20%. Furthermore, MacDonald et al. (1979) pointed out that surface rugosity of particles is of great influence on h_η , which could range from 1.8 for smooth particles to more than 4 for very rough particles.

In order to eliminate this source of uncertainty, specific experiments on monodisperse beds have been conducted in order to determine the values of h_K and h_η for the spherical particles used in that study (Table 2). Thus, best fitting values for h_K and h_η have been identified for monodisperse beds packed with 1.5 mm, 2 mm, 3 mm, 4 mm and 8 mm glass beads, in air and water flows. Results are summarized in Table 4. Ergun constants seem to differ when identified with air or water data, which could indicate that the pore-scale flow structure is different in air and water flows. However, the identified values remain within the range of literature recommendations. Besides, the Ergun law is an empirical correlation, and significant dispersions have been observed for h_K and h_η . Macdonald et al. (MacDonald et al., 1979), for example, observed that the dispersion on h_K could be greater than 50%. Since our data present a less-than-10% dispersion, we can be confident that using their mean values is relevant in that study.

Mean value for h_K is 181 ± 17 , which is in agreement with MacDonald et al. (1979), while mean value for h_η , of 1.63 ± 0.15 , is closer to recommendation of Ozahi et al. (2008). These values will be used in next paragraphs to identify equivalent diameters for non-monodisperse particle beds.

The authors point out that these values are specific to the particles used in this study, i.e., smooth particles. Although they

Table 4

Ergun constants best fitting values for each particle size. Standard deviations, which correspond to the uncertainties on the mean values, are less than 10%.

d (mm)	h_K		h_η	
	Air	Water	Air	Water
1.5	167.4 ± 5.5	196.4 ± 10.8	1.79 ± 0.01	1.41 ± 0.07
2	169.1 ± 5.8	183.1 ± 9.7	1.61 ± 0.06	1.74 ± 0.06
3	168.8 ± 4.6	175.4 ± 9.7	1.78 ± 0.11	1.60 ± 0.06
4	177.0 ± 6.1	178.6 ± 8.3	1.78 ± 0.09	1.54 ± 0.04
8	189.2 ± 27.9	206.3 ± 17.8	1.57 ± 0.07	1.46 ± 0.09
Mean	181 ± 17		1.63 ± 0.15	

present a good agreement with recommended values in literature, they should be used carefully with other classes of particles (very rough particles, for example), especially considering the dispersion reported in MacDonald et al. (1979).

4.2. Non-spherical particles beds

From various existing definitions in literature (Ozahi et al., 2008; Li and Ma, 2011b) for equivalent diameters, 4 have been identified as potentially relevant for this study:

- Volume equivalent diameter

$$d_V = \left(\frac{6V_{part}}{\pi} \right)^{1/3}; \quad (23)$$

- Surface equivalent diameter

$$d_S = \left(\frac{S_{part}}{\pi} \right)^{1/2}; \quad (24)$$

- Specific surface equivalent diameter, or Sauter diameter

$$d_{St} = \frac{6V_{part}}{S_{part}} = \frac{6V_{part}}{S_{part}}. \quad (25)$$

- Product of Sauter diameter and an adimensional sphericity coefficient, corresponding to the ratio between the surface of volume equivalent sphere and the actual surface of the particle.

$$d_{St}\psi = \frac{6V_{part}}{S_{part}} \frac{\pi^{1/3}(6V_{part})^{2/3}}{S_{part}} \quad (26)$$

4.2.1. Permeability

Identification of equivalent diameter for permeability, d_K , is done by studying the difference between experimental data in Darcy regime and prediction of Darcy's law, where permeability is calculated with Eq. (19) using d_V , d_S , d_{St} or $d_{St}\psi$ as the characteristic dimension d . This difference is normalized by the experimental pressure loss:

$$\frac{\left(-\frac{\partial P}{\partial z} + \rho g \right) (d) - \left(-\frac{\partial P}{\partial z} + \rho g \right)_{exp}}{\left(-\frac{\partial P}{\partial z} + \rho g \right)_{exp}} = \frac{\frac{\mu U}{K(d)} - \frac{\mu U}{K_{exp}}}{\frac{\mu U}{K_{exp}}} \quad (27)$$

$$= \frac{\frac{1}{K(d)} - \frac{1}{K_{exp}}}{\frac{1}{K_{exp}}}.$$

Expression (27) has been evaluated for each one of the 4 potential equivalent diameters, for each one of the 5 non-spherical particle beds considered, in air and water flows, defining 4 sets of 10 values (see left columns Table 5). Mean value and standard deviation of these sets have been determined. In order to represent these results in a more visual way, Fig. 10(a) shows Gaussian

distribution functions of corresponding mean values and standard deviation.

It can be seen in Fig. 10(a) that the Sauter diameter d_{St} is the one which allows the best prediction, on average, of pressure losses in Darcy regime, while $d_{St}\psi$ leads to underestimate them, by 24.5%, and d_V and d_S to overestimate them, by 34.2% and 55.3%, respectively. Furthermore, predictions of pressure losses using $d_{St}\psi$ and d_{St} present the lowest dispersions, which means that d_{St} allows a correct prediction not only on average but also for each tested bed individually. Indeed, it can be seen in Table 5 that this prediction always presents a less-than-16% difference with experimental data, which is very small for such an experimental correlation. Therefore, the Sauter diameter d_{St} constitutes a good equivalent diameter for permeability of non-spherical particle beds.

4.2.2. Passability

Similar procedure is used to determine the equivalent diameter for passability d_η . It is done by studying the difference between experimental deviations to Darcy's law and prediction using Eq. (20), where characteristic dimension is d_V , d_S , d_{St} or $d_{St}\psi$, normalized by experimental deviations to Darcy's law:

$$\frac{\left(-\frac{\partial P}{\partial z} + \rho g - \frac{\mu U}{K} \right) (d) - \left(-\frac{\partial P}{\partial z} + \rho g - \frac{\mu U}{K} \right)_{exp}}{\left(-\frac{\partial P}{\partial z} + \rho g - \frac{\mu U}{K} \right)_{exp}} = \frac{\frac{\rho U^2}{\eta(d)} - \frac{\rho U^2}{\eta_{exp}}}{\frac{\rho U^2}{\eta_{exp}}} \quad (28)$$

$$= \frac{\frac{1}{\eta(d)} - \frac{1}{\eta_{exp}}}{\frac{1}{\eta_{exp}}}.$$

Mean values and standard deviations of expression (28), for each potential equivalent diameter (d_V , d_S , d_{St} and $d_{St}\psi$), have been determined (see right columns of Table 5), and are represented in Fig. 10(b) by Gaussian distribution functions. Contrary to Fig. 10(a), best prediction of deviation to Darcy's law is obtained with the product of Sauter diameter and sphericity coefficient $d_{St}\psi$, which leads to a 9.0% overestimation of deviation to Darcy's law, on average, while d_{St} , d_V and d_S lead to overestimate it by 26.2%, 46.1% and 57.3%, respectively. Therefore, the product of Sauter diameter and sphericity constitutes a good choice for the equivalent diameter for passability of non-spherical particle beds.

However, it should be pointed out here that prediction of deviations to Darcy's law using this diameter is not correct for all tested beds (a 23.2% difference is observed for 5×8 mm cylinders in water flow), which suggests that this correlation would turn incorrect if the Darcy term was small compared to the quadratic one, and, therefore, that it presents a limited validity domain. Nevertheless, and looking at experimental data obtained in the present study, the use of this correlation can definitely be recommended within

Table 5
Experimental permeabilities and passabilities of non-spherical particle beds.

Particle	K_{exp} ($\times 10^{-9} m^2$)	$\frac{\frac{1}{K(d)} - \frac{1}{K_{exp}}}{\frac{1}{K_{exp}}} (%)$				η_{exp} ($\times 10^{-5} m$)	$\frac{\frac{1}{\eta(d)} - \frac{1}{\eta_{exp}}}{\frac{1}{\eta_{exp}}} (%)$				
		d_V	d_S	d_{St}	$d_{St}\psi$		d_V	d_S	d_{St}	$d_{St}\psi$	
c5 × 5	Air	16.550 ± 0.074	13.8	26.5	-7.8	-25.3	16.90 ± 0.99	40.5	48.0	26.4	13.8
	Water	15.00 ± 0.22	24.2	38.0	0.6	-18.5	17.74 ± 0.15	32.5	39.6	19.3	7.3
c5 × 8	Air	27.21 ± 0.11	41.2	62.5	6.7	-19.4	30.30 ± 0.67	32.5	42.1	15.2	0.1
	Water	17.24 ± 0.19	48.6	70.9	12.3	-15.1	17.41 ± 0.14	63.0	74.9	41.7	23.2
c8 × 12	Air	66.00 ± 0.49	35.1	53.6	4.5	-19.2	46.81 ± 0.68	26.2	34.6	11.0	-2.3
	Water	47.15 ± 0.34	48.9	69.3	15.2	-10.9	37.75 ± 0.35	27.5	36.0	12.2	-1.4
p4 × 4	Air	10.054 ± 0.040	21.7	46.5	-16.0	-42.1	12.44 ± 0.77	61.9	77.6	34.5	11.7
	Water	9.63 ± 0.18	42.8	71.9	-1.5	-32.1	13.11 ± 0.12	69.8	86.3	41.1	17.2
p6 × 6	Air	24.78 ± 0.16	20.2	41.7	-13.5	-37.8	20.9 ± 1.0	53.7	66.9	30.3	10.5
	Water	19.70 ± 0.27	45.7	71.8	4.8	-24.6	20.29 ± 0.18	53.2	66.4	30.0	10.2
	Mean		34.2	55.3	0.5	-24.5		46.1	57.3	26.2	9.0
	Standard deviation		13.1	16.4	10.4	10.0		16.2	19.3	11.3	8.3

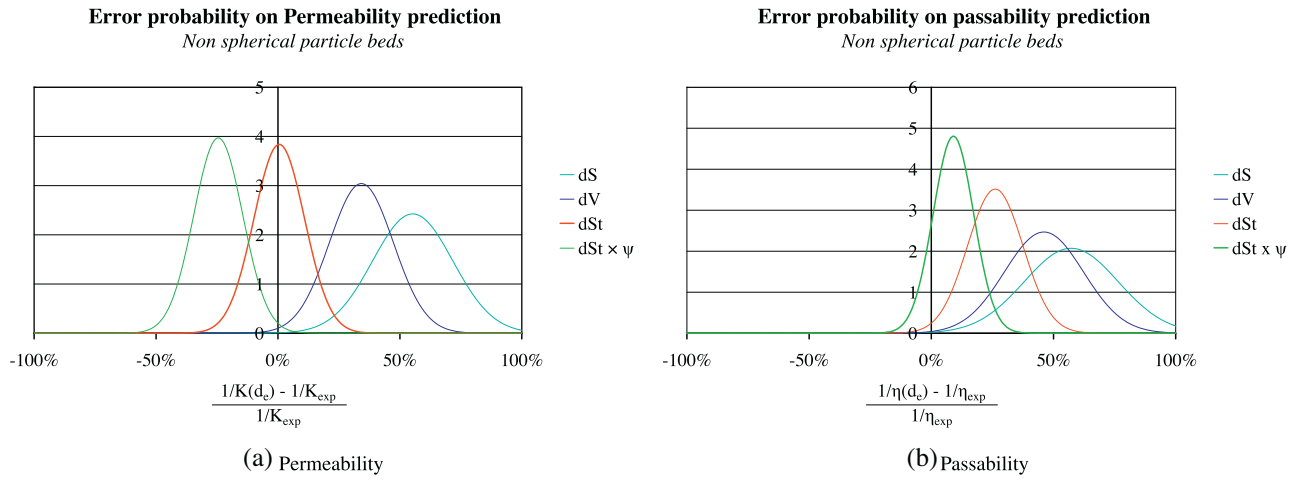


Fig. 10. Identification of equivalent diameter for non-spherical particle beds.

the investigated range of Reynolds numbers, i.e., from $Re=0$ to $Re=1500$:

$$-\frac{\partial P}{\partial z} + \rho g = \frac{h_K(1-\varepsilon)^2}{\varepsilon^3 d_{St}} \mu U + \frac{h_\eta(1-\varepsilon)}{\varepsilon^3 d_{St} \psi} \rho U^2, \quad (29)$$

where:

$$d_{St} = \frac{6V_{part}}{S_{part}} \quad (30)$$

$$\psi = \frac{\pi^{1/3}(6V_{part})^{2/3}}{S_{part}} \quad (31)$$

$$h_K = 181 \quad (32)$$

$$h_\eta = 1.63. \quad (33)$$

4.3. Multi-sized spherical particles

The objective of this paragraph is to determine mean diameters for the studied multi-sized spherical particle beds. From many definitions of mean diameters existing in the literature, 4 seem particularly interesting:

- Number mean diameter

$$d_{(n)} = \frac{\sum_i d_i n_i}{\sum_i n_i}; \quad (34)$$

- Length mean diameter

$$d_{(l)} = \frac{\sum_i d_i^2 n_i}{\sum_i d_i n_i}; \quad (35)$$

- Surface mean diameter

$$d_{(s)} = \frac{\sum_i d_i^3 n_i}{\sum_i d_i^2 n_i}; \quad (36)$$

- Volume mean diameter

$$d_{(v)} = \frac{\sum_i d_i^4 n_i}{\sum_i d_i^3 n_i}. \quad (37)$$

4.3.1. Permeability

Identification of equivalent diameters for permeability, d_K , and passability, d_η , is done by a similar method to the case of non-spherical particle beds. Expressions (27) and (28) have been evaluated for each one of the 4 potential equivalent diameters, for each one of the 4 non-spherical particle beds considered, in air and water flows (see Table 6). Fig. 11(a) summarizes results for permeability, and shows that the Surface mean diameter, $d_{(s)}$, allows the best prediction of pressure losses in Darcy regime, since it leads to slightly overestimate it by less than 4.6% on average, while the Volume mean diameter $d_{(v)}$ leads to underestimate it by 26.8%, and Length mean diameter $d_{(l)}$ and Number mean diameter $d_{(n)}$ leads to overestimate it respectively by 32.2% and 51.0%. Furthermore, predictions of pressure losses in Darcy regime corresponding to $d_{(s)}$ present the smallest dispersion, which shows that this diameter

Table 6
Experimental permeabilities and passabilities of multi-sized spherical particle beds.

Mixture	K_{exp} ($\times 10^{-9}m^2$)	$\frac{\frac{1}{K(d)} - \frac{1}{K_{exp}}}{\frac{1}{K_{exp}}} (\%)$				η_{exp} ($\times 10^{-5}m$)	$\frac{\frac{1}{\eta(d)} - \frac{1}{\eta_{exp}}}{\frac{1}{\eta_{exp}}} (\%)$				
		$d_{(n)}$	$d_{(l)}$	$d_{(s)}$	$d_{(v)}$		$d_{(n)}$	$d_{(l)}$	$d_{(s)}$	$d_{(v)}$	
1	Air	2.499 ± 0.083	50.3	34.5	0.2	-46.9	8.87 ± 0.15	22.2	15.6	-0.3	-27.3
	Water	2.402 ± 0.028	44.4	29.2	-3.8	-48.9	7.54 ± 0.33	3.9	-1.7	-15.2	-38.2
2	Air	2.512 ± 0.012	50.2	32.7	8.9	-16.6	7.532 ± 0.075	6.4	0.0	-9.4	-20.7
	Water	2.735 ± 0.038	63.5	44.5	18.5	-9.2	8.23 ± 0.32	16.3	9.3	-1.0	-13.4
3	air	5.837 ± 0.029	80.5	48.8	7.8	-31.6	13.48 ± 0.13	36.0	23.5	5.1	-16.2
	Water	5.50 ± 0.11	69.9	40.1	1.5	-35.6	13.55 ± 0.35	36.7	24.1	5.7	-15.8
4	Air	2.723 ± 0.013	34.7	23.4	9.9	-5.8	7.724 ± 0.088	-3.2	-7.4	-12.6	-19.1
	Water	2.315 ± 0.027	14.5	4.9	-6.5	-19.9	9.10 ± 0.37	14.0	9.1	3.0	-4.7
	Mean		51.0	32.2	4.6	-26.8		16.5	9.1	-3.1	-19.4
	Standard deviation		20.8	13.8	8.2	16.4		14.5	11.6	8.2	10.0

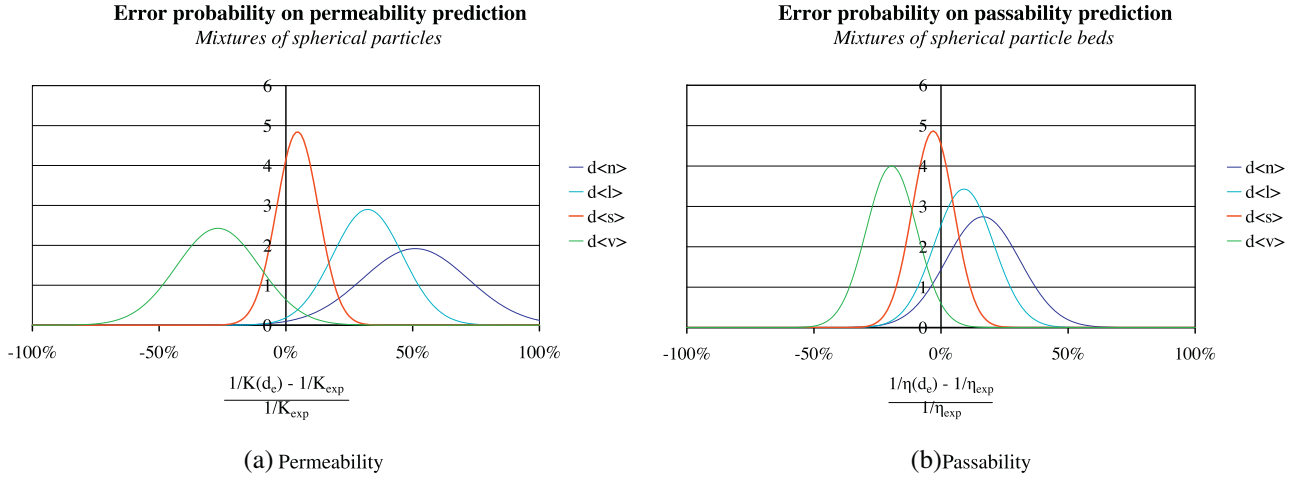


Fig. 11. Identification of equivalent diameter for multi-sized-spherical particle beds.

allows a correct prediction not only on average but also for each tested bed individually. Thus, it can be seen in Table 6 that this prediction always presents a less-than-10% difference with experimental data, except for mixture 2 in water flow, for which this difference is 18.5%, which remains reasonable. Therefore, the equivalent diameter for permeability of multi-sized spherical particle beds is the Surface mean diameter $d_{(s)}$.

4.3.2. Passability

Similar observations can be made for passability results. Mean values and standard deviations of expression (28), for each potential equivalent diameter, have been determined (see right columns of Table 6), and are represented in Fig. 11(b) by Gaussian laws. It can be seen that Surface mean diameter allows the best prediction of deviation to Darcy's law. Indeed, it leads to a slight underestimation, by 3.1%, while $d_{(v)}$ leads to underestimate it by 19.4%, and $d_{(l)}$ and $d_{(n)}$ lead to an overestimation by 9.1% and 16.5%, respectively. Furthermore, predictions of deviations to Darcy's law using this diameter present the smallest dispersion. Therefore, the equivalent diameter for passability of multi-sized spherical particle beds is the Surface mean diameter.

Thus, it has been shown at this point that pressure losses generated by non-spherical particle beds and multi-sized spherical particle beds can be accurately predicted by Ergun's law using an "equivalent diameter" approach for permeability and passability. It has been observed that equivalent diameters for permeability and passability of non-spherical particle beds are the Sauter diameter of the particles and the product of the Sauter diameter and the sphericity coefficient, respectively. The same study, on multi-sized

spherical particle beds, showed that equivalent diameters for permeability and passability of this kind of particle bed are both equal to the surface mean diameter. It is of fundamental interest here to remark that these observations are consistent: indeed, the surface mean diameter of a multi-sized spherical particle bed is equal to its Sauter diameter:

$$d_{(s)} = \frac{\sum_i d_i^3 n_i}{\sum_i d_i^2 n_i} = \frac{6 \sum_i \frac{\pi d_i^3}{6} n_i}{\sum_i \pi d_i^2 n_i} = \frac{6 \sum_i v_i n_i}{\sum_i s_i n_i} = \frac{6V_{part}}{S_{part}} = d_{St}, \quad (38)$$

and the sphericity coefficient is 1 for spherical particles.

Therefore, applicability of Eqs. (29)–(33) can be extended to all tested particle beds, i.e., both non-spherical particle beds and multi-sized spherical particle beds, and in Darcy to Weak Turbulent regime.

5. Conclusions

Motivated by uncertainty reduction in nuclear debris beds coolability, experiments have been conducted on the CALIDE facility in order to investigate single phase pressure losses in representative debris beds.

In this paper, experimental results obtained on the CALIDE facility have been presented and analyzed in order to identify a simple single-phase flow pressure loss correlation for debris-bed-like particle beds covering various reflooding flow conditions.

On the basis of current literature, Reynolds number in single-phase parts of a nuclear debris bed was estimated to range from $Re = 15$ to more than $Re = 1000$, and debris bed granulometry was

estimated between a few hundreds microns to 10 mm, with convex high sphericity shapes and porosity of the order of 40%.

Experimental data obtained on the CALIDE facility have been interpreted to determine the macro-scale behavior of pressure losses in particle beds. It was observed that a Darcy–Forchheimer law, involving the sum of a linear term and a quadratic term, with respect to fluid velocity, was relevant to describe this behavior in Darcy, Inertial and Weak Turbulent regimes. It has also been observed that, in a restricted domain between Darcy and Inertial regimes, deviation to Darcy's law is better described by a cubic term. This corresponds to the so-called Weak Inertial regime, which can be theoretically derived from pore-scale Navier-Stokes equations, and reproduced in numerical simulations, but has never been observed experimentally, to our knowledge, on disordered porous media. Nevertheless, it was pointed out that Weak Inertial deviation is very small compared to Darcy term, and, therefore, that Darcy–Forchheimer law remains relevant even in the Weak Inertial regime.

Darcy–Forchheimer law allowing a qualitative description of pressure losses only, it was necessary to determine expressions for coefficients of linear and quadratic terms in order to obtain a predictive correlation. Applicability of the Ergun's law, which is valid for monodisperse particle beds only, was investigated by assessing the possibility to define equivalent diameters for the studied beds. This approach has been found to be relevant for both permeability and passability prediction. It was observed that permeabilities of all tested beds, i.e., non-spherical and multi-sized spherical particle beds, could be precisely predicted, by less than 10% in most cases, by Ergun expression using the Sauter diameter, while the product of the Sauter diameter and the sphericity coefficient ψ allowed for an accurate prediction of passabilities, by about 15%.

Therefore, the following correlation can be recommended for calculation of single-phase pressure losses in nuclear debris beds during reflooding, for Reynolds numbers ranging from 0 to 1500:

$$-\frac{\partial P}{\partial z} + \rho g = \frac{181(1-\varepsilon)^2}{\varepsilon^3 d_{St}} \mu U + \frac{1.63(1-\varepsilon)}{\varepsilon^3 d_{St} \psi} \rho U^2, \quad (39)$$

Appendix A. Effect of gas compressibility

In air flows, the density is a function of pressure. The perfect gas hypothesis states:

$$\rho = \frac{P}{rT}, \quad (40)$$

where P is the absolute pressure, T the absolute temperature and r the specific gas constant, which is equal to 287 for air. Thus, the pressure losses along the test section are causing drops of the gas density and velocity. When compressibility effects are taken into account, the Ergun equation can be re-written as:

$$-\frac{dP}{dz} = \frac{\mu}{K} \frac{\dot{m}}{\rho(P)\pi D^2/4} + \frac{\rho(P)}{\eta} \left(\frac{\dot{m}}{\rho(P)\pi D^2/4} \right)^2 \quad (41)$$

$$\Leftrightarrow -\rho(P)dP = \left[\frac{\mu}{K} \frac{\dot{m}}{\pi D^2/4} + \frac{1}{\eta} \left(\frac{\dot{m}}{\pi D^2/4} \right)^2 \right] dz \quad (42)$$

$$\Leftrightarrow -\frac{P}{rT} dP = \left[\frac{\mu}{K} \frac{\dot{m}}{\pi D^2/4} + \frac{1}{\eta} \left(\frac{\dot{m}}{\pi D^2/4} \right)^2 \right] dz, \quad (43)$$

where \dot{m} is the mass flow rate, which is constant along the test section. By introducing the perfect gas hypothesis, we get:

Integration of Eq. (43) over the column height leads to:

$$-\int_{P_1}^{P_2} \frac{P}{rT} dP = \int_{z_1}^{z_2} \left[\frac{\mu}{K} \frac{\dot{m}}{\pi D^2/4} + \frac{1}{\eta} \left(\frac{\dot{m}}{\pi D^2/4} \right)^2 \right] dz \quad (44)$$

$$\Rightarrow -\frac{1}{2rT} \underbrace{(P_2^2 - P_1^2)}_{(P_2 - P_1)(P_1 + P_2)} = H \left[\frac{\mu}{K} \frac{\dot{m}}{\pi D^2/4} + \frac{1}{\eta} \left(\frac{\dot{m}}{\pi D^2/4} \right)^2 \right] \quad (45)$$

$$\Leftrightarrow -\Delta P \underbrace{\frac{P_1 + P_2}{2rT}}_{\rho \left(\frac{P_1 + P_2}{2} \right) = \bar{\rho}} = H \left[\frac{\mu}{K} \frac{\dot{m}}{\pi D^2/4} + \frac{1}{\eta} \left(\frac{\dot{m}}{\pi D^2/4} \right)^2 \right] \quad (46)$$

$$\Leftrightarrow -\frac{\Delta P}{H} = \underbrace{\frac{\mu}{K} \frac{\dot{m}}{\bar{\rho}\pi D^2/4}}_{U(\bar{\rho})} + \underbrace{\frac{1}{\eta} \left(\frac{\dot{m}}{\bar{\rho}\pi D^2/4} \right)^2}_{U(\bar{\rho})^2} \quad (47)$$

Therefore, compressibility effects are taken into account by calculating the gas density at the average pressure $\frac{P_1 + P_2}{2}$. The authors would like to point out that this correction has a very weak impact in this work, since the pressure loss magnitude is of a few millibars at maximum, which is very small compared to the atmospheric pressure. However, compressibility effects would play a significant role if pressure losses were not small compared to the absolute pressure of the system (higher columns, greater velocities . . .)

References

- Akers, D., Carlson, E., Cook, B., Ploger, S., Carlson, J., 1986. TMI-2 Core Debris Grab Samples – Examination and Analysis. Tech. Rep. Sandia National Laboratory, GEND-INF-075.
- Atkhen, K., Berthoud, G., 2006. SILFIDE experiment: coolability in a volumetrically heated debris bed. *Nucl. Eng. Des.* 236, 2126–2134.
- Broughton, J., Kuan, P., Petti, D., Tolman, E., 1989. A scenario of the three mile island unit-2 accident. *Nucl. Technol.* 87, 34–53.
- Bürger, M., Buck, M., Schmidt, W., Widmann, W., 2006. Validation and application of the WABE code: investigations of constitutive laws and 2D effects on debris coolability. *Nucl. Eng. Des.* 236, 2164–2188.
- Chauveteau, G., Thirriot, C., 1967. Régimes d'écoulement en milieu poreux et limite à la loi de Darcy. *Houille Blanche* 2, 141–148.
- Chikhi, N., 2014. First experimental results of large scale debris bed reflood tests in the PEARL facility. In: 16th International Topical Meeting on Nuclear Reactor Thermalhydraulics (NURETH 16).
- Chikhi, N., Coindreau, O., Li, L., Ma, W., Taivassalo, V., Takasuo, E., Leininger, S., Kulenovic, R., Laurien, E., 2014. Evaluation of an effective diameter to study quenching and dry-out of complex debris bed. *Ann. Nucl. Energy* 74, 24–41.
- Coindreau, O., Fichot, F., Fleuret, J., 2013. Nuclear fuel rod fragmentation under accident conditions. *Nucl. Eng. Des.* 255, 68–76.
- du Plessis, J., Woudberg, S., 2008. Pore scale derivation of the Ergun equation to enhance its adaptability and generalization. *Chem. Eng. Sci.* 63, 2576–2586.
- Durin, T., Rahni, N., Guigueno, Y., Raimond, E., 2013. L2 PSA development and review activities of IRSN in the framework of the 3rd PSR of the French 1300 MWe PWR series. In: International Topical Meeting on Probabilistic Safety Assessment and Analysis 2013, PSA 2013, vol. 3, pp. 2434–2445.
- Dybbes, A., Edwards, R., 1984. A new look at porous media mechanics – Darcy to Turbulent. In: Fundamentals of Transport Phenomena in Porous Media. M. Nijhoff, pp. 199–254.
- Ergun, S., 1952. Fluid flow through packed columns. *Chem. Eng. Progr.* 48 (2), 89–94.
- Firdaouss, M., Guermont, J., Le Quééré, P., 1997. Non linear corrections to Darcy's law at low Reynolds numbers. *J. Fluid Mech.* 343, 331–350.
- Forchheimer, P., 1901. Wasser Bewegung durch Boden. *Z. Ver. Dtsch. Ing.* 45, 1782–1788.
- Ginsberg, T., Klein, J., Klages, J., Sanborn, Y., Schwarz, C., Chen, J., Wei, L., 1986 January. Experimental and Analytical Investigation of Quenching of Superheated Debris Beds Under Top-Reflood Conditions. Final Report.
- Hobbins, R., McPherson, G., 1990. A summary of results from the LOFT LP-FP-2 test and their relationship to other studies at the Power Burst Facility and of the Three Mile Island Unit-2 accident. In: LOFT Open Forum, Madrid, Spain.
- Huhtiniemi, I., Magallon, D., 1999. Insight into steam explosions with corium melts in KROTOS. In: 9th International Topical Meeting on Nuclear Reactor Thermal-Hydraulics, NURETH-9, San Fransisco, USA.
- Huhtiniemi, I., Magallon, D., Hohmann, H., 1997. Results of recent KROTOS FCI tests: alumina vs corium melts. In: OECD/CSNI Specialists Meeting on Fuel-Coolant Interactions, Tokai-Mura, Japan.

- Kuwahara, F., Kameyama, Y., Yamashita, S., Nakayama, A., 1998. Numerical model of turbulent flow in porous media using a spatially periodic array. *J. Porous Media* 1, 47–55.
- Lasseux, D., Abbasian, A., Ahmadi, A., 2011. On the stationary macroscopic inertial effects for one-phase flow in ordered and disordered porous media. *Phys. Fluids*, 23.
- Lasseux, D., Ahmadi, A., Arani, A., 2008. Two-phase inertial flow in homogeneous porous media: a theoretical derivation of a macroscopic model. *Transp. Porous Media* 75, 371–400.
- Latifi, M.A., Midoux, N., Storck, A., Gence, J.N., 1989. The use of micro-electrodes in the study of the flow regime in a packed bed reactor with single phase liquid flow. *Chem. Eng. Sci.* 44, 2501–2508.
- Li, L., Ma, W., 2011a. Experimental characterization of the effective particle diameter of a particulate bed packed with multi-diameter spheres. *Nucl. Eng. Des.* 241, 1736–1745.
- Li, L., Ma, W., 2011b. Experimental study on the effective particle diameter of a packed bed with non-spherical particles. *Transp. Porous Media* 89, 35–48.
- Lide, D., 1990. *CRC Handbook of Chemistry and Physics*, 70th edn. CRC Press, Boca Raton, FL.
- Ma, W., Dinh, T.-N., 2010. The effects of debris bed's prototypical characteristics on corium coolability in a LWR severe accident. *Nucl. Eng. Des.* 240, 598–608.
- MacDonald, I., El-Sayed, M., Mow, K., Dullien, F., 1979. Flow through porous media – the Ergun equation revisited. *Ind. Eng. Chem. Fundam.* 18, 199–208.
- MacDonald, M., Chu, C., Guilloit, P., Ng, K., 1991. A generalized Blake-Kozeny equation for multisized spherical particles. *AIChE J.* 37 (10), 1583–1588.
- Magallon, D., Huhtiniemi, I., 2001. Corium melt quenching tests at low pressure and subcooled water in FARO. *Nucl. Eng. Des.* 204, 369–376.
- Mei, C., Auriault, J., 1991. The effect of weak inertia on flow through a porous medium. *J. Fluid Mech.* 222, 647–663.
- Nemec, D., Levec, J., 2005. Flow through packed bed reactors: 1. Single phase flow. *Chem. Eng. Sci.* 60, 6947–6957.
- Oguma, M., 1983. Cracking and relocation behavior of nuclear fuel pellets during rise to power. *Nucl. Eng. Des.* 76, 35–45.
- Olander, D., 1990. *Fundamental Aspects of Nuclear Reactor Fuel Elements*. US-DOE Report, TID-26711-P1.
- Ozahi, E., Gundogdu, M.-Y., Carpinlioglu, M.-Ö., 2008. A modification on Ergun's correlation for use in cylindrical packed beds with non-spherical particles. *Adv. Powder Technol.* 19, 369–381.
- Petti, D., Martinson, Z., Hobbins, R., Allison, C., Carlson, E., Hargman, D., Cheng, T., Hartwell, J., Vinjamuri, K., Seifken, L., 1989. Power Burst Facility (PBF) Severe Fuel Damage Test: 1–4 Test Result Report, U.S. Nuclear Regulatory Commission NUREG/CR-5163, EGG-2542.
- Rashid, M., Chen, Y., Kulenovic, R., Laurien, E., 2008. Experiments on the coolability of a volumetrically heated particle bed with irregularly shaped particles. In: 7th International Meeting on Nuclear Reactor Thermal Hydraulics Operation and Safety, NUTHOS-7, Seoul, Korea, October 5–9.
- Repetto, G., 1990. Rapport définitif de dépouillement de l'essai B9R et résultats complémentaires de l'essai B9. Tech. Rep. PHEBUS CSD 118/90, CEA.
- Repetto, G., Chikhi, N., Fichot, F., 2013. Main outcomes on debris bed cooling from PRELUDE experiments. In: 6th European Review meeting on Severe Accident Research, ERMSAR-2013.
- Repetto, G., Garcin, T., Eymery, S., Fichot, F., 2011. Experimental program on debris reflood (PEARL) – results on PRELUDE facility. *Nucl. Eng. Des.* 264, 176–186.
- Shaban, H., Khan, A., 1995. Pressure-related operational problems and their remedies in hydrotreating reactors in petroleum refineries. *J. Pet. Sci. Eng.* 14, 79–88.
- Soulaine, C., Quintard, M., 2014. On the use of Darcy–Forchheimer like model for a macro-scale description of turbulence in porous media and its application to structured packings. *Int. J. Heat Mass Transf.* 74, 88–100.
- Spencer, B., Wang, K., Blomquist, C., McUmbler, L., Schneider, J., 1994. Fragmentation and Quench Behaviour of Corium Melt Streams in Water, US Nuclear Regulatory Commission, NUREG/CR-6133, ANL-93/92.
- Tutu, N., Ginsberg, T., Klein, J., Klages, J., Schwarz, C., 1984. Debris Bed Quenching Under Bottom Flood Conditions (In-Vessel Degraded Core Cooling Phenomenology) [PWR]. Tech. Rep. Brookhaven National Lab.
- Wang, C., Dhir, V., 1988. An experimental investigation of multidimensional quenching of a simulated core debris bed. *Nucl. Eng. Des.* 110, 61–72.
- Wodié, J., Levy, T., 1991. Correction non linéaire à la loi de Darcy. *C. R. l'Acad. Sci. Paris t.312, Sér. II*, 157–161.
- Yazdchi, K., Luding, S., 2012. Toward unified drag laws for inertial flows through fibrous media. *Chem. Eng. J.* 207, 35–48.